Inorg. Chem. **2008**, *47*, 5190−5196

Functionalized Europium Nanorods for In Vitro Imaging

Ka-Leung Wong,[†] Ga-Lai Law,[‡] Margaret B. Murphy,[†] Peter A. Tanner,[†] Wing-Tak Wong,[‡] Paul Kwan-Sing Lam,[†] and Michael Hon-Wah Lam*[,†]

Department of Biology and Chemistry, City University of Hong Kong, Tat Chee Avenue, Kowloon Tong, Hong Kong, and Department of Chemistry, The University of Hong Kong, Pokfulam, Hong Kong

Received January 10, 2008

Emissive europium hydroxide nanorods (ENR) (20 nm × 500 nm) functionalized by a surface coating of chromophore-containing organically modified silicate (ORMOSIL) layer, have been synthesized and characterized by high-resolution transmission electron microscopy (TEM). Low-temperature photophysical characterization of the functionalized nanorods (FENR) demonstrated a strong red $^5D_0$ luminescence both in solid and in suspended solutions. Potentials of this nanorod material for live cell imaging have also been explored. Both the bare and functionalized nanorods are able to enter living human cells with no discernible cytotoxicity. Chromophore-to-Eu^{3+} energy-transfer in the functionalized nanorods enables staining of the cytoplasm of living human cells. This is confirmed by costaining with fluorescent dextran. The red chromophore-sensitized luminescence from the internalized nanorods in live human lung carcinoma cells (A549) can be observed by confocal microscopy 2 h after loading and reaches maximal emission after 24 h.

Introduction

Because of their intriguing photophysical properties, biomedical applications of luminescent lanthanide complexes have attracted increasing attention in recent years.[1–5] Their unique characteristics, such as long luminescent lifetime, large Stokes shift, and narrow peak width of emission bands, render these complexes useful as luminescent labels, probes, and sensors for time-resolved fluorometric assays, immunoassays, and ultrasensitive in vitro and in vivo imaging.[6–9] Besides molecular lanthanide chelates, potential applications of lanthanide-doped and lanthanide-based nanomaterials have also been actively explored.[10–13] This is mainly because of their additional advantageous features, such as low intrinsic cytotoxicity,[14] ability to effect up-conversion,[15–17] and convenience in surface functionalization by biomolecules for fluorescent labeling,[18–20] which make them attractive alternatives to quantum dots. Up to now, many of the nanolanthanide luminescent probes in the literature are based on doped lanthanide phosphors and nanocrystals with selected lanthanide ions embedded in crystalline or sol−gel host

* To whom correspondence should be addressed. E-mail: bhmhwlam@cityu.edu.hk. Phone: 852-27887329.
[†] Department of Biology and Chemistry, City University of Hong Kong.
[‡] Department of Chemistry, The University of Hong Kong.

(1) Yuan, J.; Wang, G.; Majima, K.; Matsumoto, K. *Anal. Chem.* **2001**, *73*, 1869.
(2) Hemmilá, I.; Mukkala, V.-M. *Crit. Rev. Clin. Lab. Sci.* **2001**, *38*, 441.
(3) Piszczek, G.; Gryczynski, I.; Maliwal, B. P.; Lakowicz, J. R. *J. Fluoresc.* **2002**, *12*, 15.
(4) Parker, D.; Dickins, R. S.; Puschmann, H.; Crossland, C.; Howard, J. A. K. *Chem. Rev.* **2002**, *102*, 1977.
(5) Nitz, M.; Sherawat, M.; Franz, K. J.; Peisach, E.; Allen, K. N.; Imperiali, B. *Angew. Chem. Int. Ed.* **2004**, *43*, 3682.
(6) Bornhop, D. J.; Hubbard, D. S.; Houlne, M. P.; Adair, C.; Kiefer, G. E.; Pence, B. C.; Morgan, D. L. *Anal. Chem.* **1999**, *71*, 2607.
(7) Scorlias, A.; Bjartell, A.; Lilja, H.; Moller, C.; Diamandis, E. P. *Clin. Chem.* **2000**, *46*, 1450.
(8) Aspinal, H. C. *Chem. Rev.* **2002**, *102*, 1807.
(9) (d) Manning, H. C.; Griffin, J. M. M.; Goebel, T. S.; Wegiel, M. A.; Thompson, R. C.; Price, R. R.; Bornhop, D. J. *Bioconjugate Chem.* **2004**, *15*, 1488.
(10) Gordon, W. O.; Carter, J. A.; Tissue, B. M. *J. Lumin.* **2004**, *108*, 339.
(11) Prodi, L. *New J. Chem.* **2005**, *29*, 20.
(12) Lim, S. F.; Riehn, R.; Ryu, W. S.; Khanarian, N.; Tung, C.-K.; Tank, D.; Austin, R. H. *Nano Lett.* **2006**, *6*, 169.
(13) Goldys, E. M.; Drozdowicz-Tomsia, K.; Jinjun, S.; Dosev, D.; Kennedy, I. M.; Yatsunenko, S.; Godlewski, M. *J. Am. Chem. Soc.* **2006**, *128*, 14498.
(14) Palmer, R. J.; Butenhoff, J. L.; Stevens, J. B. *Environ. Res.* **1987**, *43*, 142.
(15) Auzel, F.; Pecile, D.; Morin, D. *J. Electrochem. Soc.* **1975**, *122*, 101.
(16) Auzel, F. *Chem. Rev.* **2004**, *104*, 139.
(17) Corstiens, P. L. A. M.; Li, S.; Zuiderwijk, M.; Kardos, K.; Abrams, W. R.; Niedbala, R. S.; Tanke, H. J. *IEEE Proc. Nanobiotechnol.* **2005**, *152*, 64.
(18) Beaurepaire, E. E.; Buissette, V.; Sauviat, M.-P.; Giaume, D.; Lahlil, K.; Mercuri, A.; Casanova, D.; Huignard, A.; Martin, J.-L.; Gacoin, T.; Boilot, J.-P.; Alexandrou, A. *Nano Lett.* **2004**, *4*, 2079.
(19) Wang, F.; Zhang, Y.; Fan, X.; Wang, M. *Nanotechnol.* **2006**, *17*, 1527.
(20) Wang, F.; Chatterjee, D. K.; Li, Z.; Zhang, Y.; Fan, X.; Wang, M. *Nanotechnology* **2006**, *17*, 5786.

10.1021/ic8000416 CCC: $40.75
Published on Web 05/21/2008

matrices.[21,22] There are only few examples of fluorescent biolabels that are based upon luminescent lanthanide-based nanomaterials. Feng et al.[23] reported the use of silica-coated and functionalized Eu_2O_3 nanoparticles as a fluorescent label for immunoassay. Patra et al.[24] reported the application of luminescent lanthanide orthophosphate $LnPO_4 \cdot H_2O$ (Ln = Eu and Tb) nanorods in live cell imaging. As a matter of fact, lanthanide-based nanomaterials are stable and are easy to fabricate and functionalize. They can readily be internalized by cells and generally exhibit no apparent detrimental effect on cell viability. Thus, besides biolabeling, they are also good candidates for in vitro and in vivo targeted drug/gene delivery vehicles.

Despite the above attractive features, the forbidden nature of $4f^N-4f^N$ transitions of lanthanide ions has nevertheless limited the brightness of lanthanide-based biolabels for cell imaging. Antenna-lanthanide ion energy transfer is an effective way to improve the quantum efficiency of lanthanide materials.[25,26] Herein, we report the synthesis and live human cell internalization of europium hydroxide nanorods. Whereas the bare nanorods already possess adequate quantum efficiency for imaging purposes by fluorescence and confocal fluorescence microscopy, surface functionalization by an organically modified silicate (ORMOSIL) coating with phenoxybenzoate as the energy-transfer antenna was found to greatly enhance the red $4f^6 - 4f^6$ emission of the nanorods.

Experimental Section

Synthesis of the Europium Hydroxide Nanorods. Europium chloride (Strem, 99.99%) (0.25 g) was added to 6 mL of H_2O and was heated to 60 °C with stirring for 10 min. The solution was transferred to a Teflon-lined digestion bomb, sealed, and heated at 140 °C for 24 h. The content in the digestion bomb was then cooled at a rate of 10 °C h^{-1} to 40 °C. The white powder obtained was washed with dilute NaOH. Yield 50%. For brevity, we label the europium hydroxide nanorods as ENR in the following.

Synthesis of ORMOSIL Precursor. Methyl 2-phenoxybenzoate (Lancaster, 98%) (0.2 g, 7.8 mmol) and 3-aminopropyltriethoxysilane (Adlrich, 98%) (0.2 g, 7.8 mmol) were mixed together in methanol and refluxed for 12 h at 70 °C. Yield: 66%; FAB-MS 460; Anal. Calcd: $C = 57.50$, $H = 5.48$, $N = 3.05$; Found: $C = 57.45$, $H = 5.43$, $N = 3.09$; δ^1H NMR (400 MHz, $CDCl_3$, 25 °C): 1.28 (m, 2H, CH_2), 1.66 (m, 2H, CH_2), 2.56 (m, 2H, CH_2), 3.67 (s, 9H, CH_3), 6.84 (d, 1H, ArH), 6.90 (t, 1H, ArH), 6.98 (t, 1H, ArH), 7.14 (t, 2H, ArH), 7.22 (t, 2H, ArH), 7.22 (d, 1H, ArH), 7.95 (d, 1H, ArH).

Surface Functionalization of Europium Hydroxide Nanorods. The ORMOIL precursor (0.2 g) was stirred with ENR (0.2 g) for 30 min with a few drops of concentrated ammonia solution in 120 mL of ethanol. The functionalized nanorods were dried in air, washed with methanol, and examined by high resoution TEM with EDX. The functionalized nanorods are labeled as FENR in the following.

Cell Culture and Nanorod Exposure. Human lung carcinoma A549 cells were purchased from the American type Culture Collection (ATCC) (#CCL-185, ATCC, Manassas, VA, USA). Cells were cultured in Ham's F12K medium with L-glutamine and phenol red (N3520, Sigma, St. Louis, MO, USA) supplemented with 10% fetal bovine serum at 37 °C and 5% CO_2. Cells were passaged every 3−5 days. Human cervical carcinoma (HeLa) cells were maintained in an RMPI 1640 medium supplemented with 10% fetal bovine serum (FBS) and 1% penicillin and streptomycin in 5% CO_2. For nanorod exposures, cells diluted 1:2 to 1:4 were plated onto 6-well plates (#140615, Nunc, Rochester, NY, USA) at 2 mL $well^{-1}$ or onto 60 × 15 mm culture dishes at 3 mL per dish. One sterile 18 × 18 mm glass coverslip was placed in each of the plate wells or in the dish before the cells were added. Cells were allowed to attach overnight. The cell medium in each well was changed immediately prior to the initiation of exposures. Stock solutions of 200−300 μg ml^{-1} ENR or FENR, as well as commerically available powder $Eu(OH)_3$ (Strem), were freshly prepared before each exposure in sterile supplemented medium and sonicated at room temperature for 30 min prior to being added to the cells. Stock solutions were also gently agitated by hand before dosing to ensure even dispersal of the nanorods or $Eu(OH)_3$ in solution. Stock solutions were added to the cells at 1:10 dilutions in supplemented medium. After exposure, the medium was removed, cells were washed two to three times with sterile PBS, and the coverslip was removed from the well or dish and mounted on a clean glass slide for imaging.

The cell growth rate was measured using a 3-(4,5-dimethyl thiazol-2-yl)-2,5-diphenyl tetrazolium bromide (MTT) proliferation assay kit according to the manufacturer's instructions (Roche Diagnostics). Briefly, 3000 cells were seeded in 96-well plates and cultured in 5% FCS for 24 h. Taxol (0, 10, 20, 30, and 40 mg ml^{-1}) was added 24 h after plating, and cell viability was examined at the 24 h postexposure time point. Before testing, 10 μl of MTT labeling reagent (5 mg ml^{-1} MTT in PBS) were added, and the cells were incubated for a further 4 h at 37 °C. Then, 100 μl of solubilizing reagent (10% SDS in 0.01 mol l^{-1} HCl) were added, and the plate was incubated overnight at 37 °C to dissolve the formazan crystals. The absorbance was measured at a wavelength of 570 nm on a Labsystem multiscan microplate reader (Merck Eurolab, Dietikon, Schweiz). Each time point was done in triplicate wells, and each experiment was repeated at least twice.

Photophysical Measurements. Low-temperature (10 K) luminescence spectra were obtained by exciting samples with a Continuum Nd:YAG laser coupled to an optical parametric oscillator (OPO). Sample emissions were dispersed through an Acton 0.5 m monochromator with a 1200 g mm^{-1} grating blazed at 500 nm and detected by a back-illuminated SpectruMM CCD detector. Samples were housed in an Oxford Instruments closed cycle cryostat system, with a base temperature of 10 K.

Room-temperature spectra were obtained by exciting the samples with an argon ion laser at 457.9 nm with a maximum power of 15 mW. Sample emissions were dispersed by a monochromator and were detected by a cooled R636−10 Hamamatsu photomultiplier in combination with a lock-in amplifier system. Emission spectra were also obtained by the exciting samples with an xenon lamp at 390 nm in a PerkinElmer LS50B Spectrofluorimeter. UV−vis absorption spectra were recorded using an HP UV-8453 spectrophotometer to measure the range between 200 and 1100 nm.

(21) Jüstel, T.; Nikol, H.; Ronda, C. *Angew. Chem., Int. Ed.* **1998**, *37*, 3084.
(22) Buissette, V.; Giaume, D.; Gacoin, T.; Boilot, J.-P. *J. Mater. Chem.* **2006**, *16*, 529.
(23) Feng, J.; Shan, G.; Maquieira, A.; Koivunen, M. E.; Guo, B.; Hammock, B. D.; Kennedy, I. M. *Anal. Chem.* **2003**, *75*, 5282.
(24) Patra, C. R.; Bhattacharya, R.; Patra, S.; Basu, S.; Mukherjee, P.; Mukhopadhyay, D. *J. Nanobiotechnol.* **2006**, *4*, 11.
(25) Wong, K.-L.; Law, G.-L.; Kwok, W.-M.; Phillips, D. L.; Wong, W.-T. *Angew. Chem., Int. Ed.* **2005**, *44*, 3436.
(26) Law, G.-L.; Wong, K.-L.; Kwok, W.-M.; Wong, W.-T.; Tanner, P. A. *J. Phys. Chem. B.* **2007**, *111*, 10858.

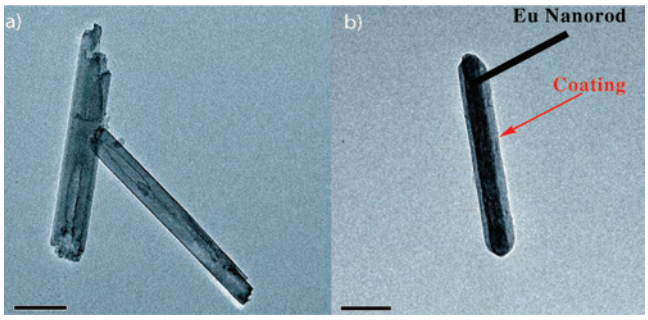

Figure 1. (a) TEM image of the hydrothermally synthesized ENR (bar = 100 nm); (b) ENR functionalized by an ORMOSIL coating (bar = 50 nm).

Confocal fluorescence microscopy was carried out using a Carl Zeiss 210 confocal microscope (Oberkochen, Germany) with 20× and 40× oil-immersion lenses, in conjunction with an argon ion laser (457.9 nm excitation). Emitted radiation was passed through a 515 nm long-pass filter. Emission spectra were collected by a lambda system from a Carl Zeiss 510 confocal microscope with a 60× oil-immersion lens. Zeiss fluorescence microscopy with a 40× oil-immersion lens, in conjuction with a xenon lamp (390 nm excitation), was used for the cell imaging of FENR.

A transmission electron microscope (TEM) (Philips, Tecnai 20), equipped with an energy-dispersive X-ray spectrometer (EDX; Hitachi HF-2000), was used to characterize the morphology, structure, and chemical properties of the nanorods. The operating voltage of the microscope was 200 kV. To obtain TEM images, the powder was dispersed in 2-propanol by ultrasonication for 10 min followed by deposition onto a copper−carbon grid. The loading and atomic compositions of the nanorods were analyzed by EDX. Nanorod morphology inside human cells was demonstrated by a Philips TEM (EM 208s) dedicated to biological applications and equipped with image analysers at 80 kV.

Results and Discussion

The synthesis of lanthanide nanowires and nanorods by various approaches, such as sonication, has been reported previously.[27,28] Our europium hydroxide nanorods (ENR) were readily prepared by a hydrothermal method from europium chloride (Figure 1). The morphology of the nanorods (20 × 500 nm) examined by TEM is shown in part a of Figure 1. A high-resolution TEM (HRTEM) image, powder diffraction pattern, and EDX spectra of the nanorod materials are presented in Figure S1 of the Supporting Information.

The fabricated ENR materials were characterized by spectroscopic techniques. The FTIR spectrum of the neat nanorods (Figure 2) is similar to that of $Y(OH)_3$ nanotubes[29] and shows two prominent bands at 3609 and 707 cm^{-1} attributable the to the stretching of O−H and deformation of Eu−OH, respectively. These bands fingerprint the crystal space group of the nanorods as pure hexagonal $P6_3/m$.

The surface of the ENR was functionalized by a coating of phenoxybenzoate chromophore-containing ORMOSIL

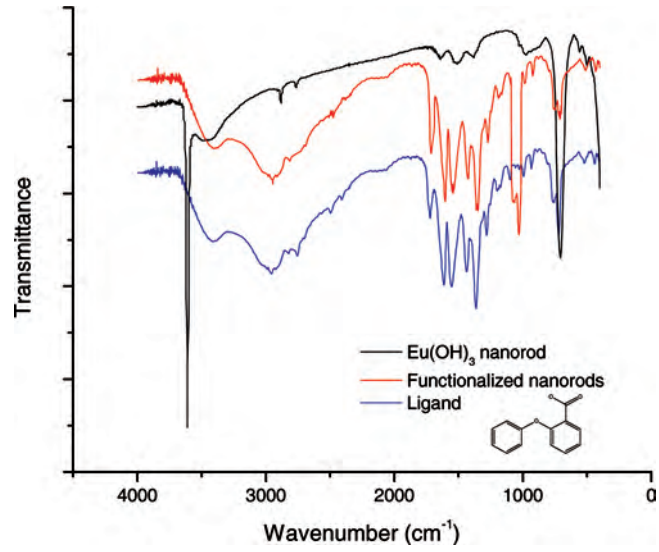

Figure 2. Room-temperature FTIR KBr disk spectra of the ENR (black line), FENR (red line), and methyl 2-phenoxybenzoate ligands (blue line).

layer via a conventional sol−gel process. The precursor of the ORMOSIL coating was prepared from aminopropyltriethoxysilane and methyl phenoxybenzoate (Scheme 1). Formation of the surface coating on the ENR was confirmed by TEM (part b of Figure 1) and EDX examination (Figure S2, Supporting Information). The thickness of the coating was ca. 5 nm. Dispersibility of the ENR in water has improved with the silane-based coating. As shown in Figure 2, FTIR spectra of the functionalized europium hydroxide nanorods (FENR) (red line) are very different from that of the ENR (black line). The prominent bands of the ENR at 3609 and 707 cm^{-1} disappear in the FENR. The region between 1608 and 1504 cm^{-1} in the latter spectrum comprises aromatic ring stretching and asymmetric carboxylate modes, whereas bands at 1093 and 1036 cm^{-1} correspond to Si−O stretching.

A sensitive test of the phase purity of the nanorods is afforded by site-selective low-temperature luminescence. Indeed, hexagonal $Eu(OH)_3$ is rather unique. Because of the C_{3h} site symmetry of Eu^{3+}, there are only three sharp emission bands in the region of the red luminescence $^5D_0 \rightarrow {}^7F_{0,1,2}$. These correspond to the three sharp features in part b of Figure 3. The higher energy emissions from $^5D_1$ and $^5D_2$ in $Eu(OH)_3$ are quenched by nonradiative relaxation to $^5D_0$ due to the high energy OH phonons. However, it is apparent from the low-temperature emission spectra (parts a−c of Figures 3) that another impurity phase is present in the ENR and under the appropriate excitation wavelength (465 nm, part c of Figure 3), the emission spectrum of this phase was recorded. The figure shows that the total degeneracies of the terminal multiplet terms are removed so that 1, 3, and 5 bands are resolved for the transitions from $^5D_0$ to $^7F_0$, $^7F_1$, and $^7F_2$, respectively. This indicates a site symmetry with, at most, a 2-fold rotation axis for Eu^{3+}. However, the considerable breadth of the bands is indicative of a disordered system, just as for Eu^{3+} in porous γ-aluminum oxide where a very similar structure is observed in the emission spectrum.[30] In fact, a literature search uncovered the emission spectrum of

(27) Pol, G.; Palchik, O.; Gedanken, A.; Felner, I. *J. Phys. Chem. B* **2002**, *106*, 9737.
(28) Mahalingham, A.; Onclin, S.; Peter, M.; Ravoo, B. J.; Huskens, J.; Reinherdt, D. N. *Langumir* **2004**, *20*, 11756.
(29) Tang, Q.; Liu, Z.; Li, S.; Zhang, S.; Liu, X.; Qian, Y. *J. Cryst. Growth* **2003**, *259*, 208.

Scheme 1. Surface Functionalization of ENR with Chromophore-ORMOSIL Coating

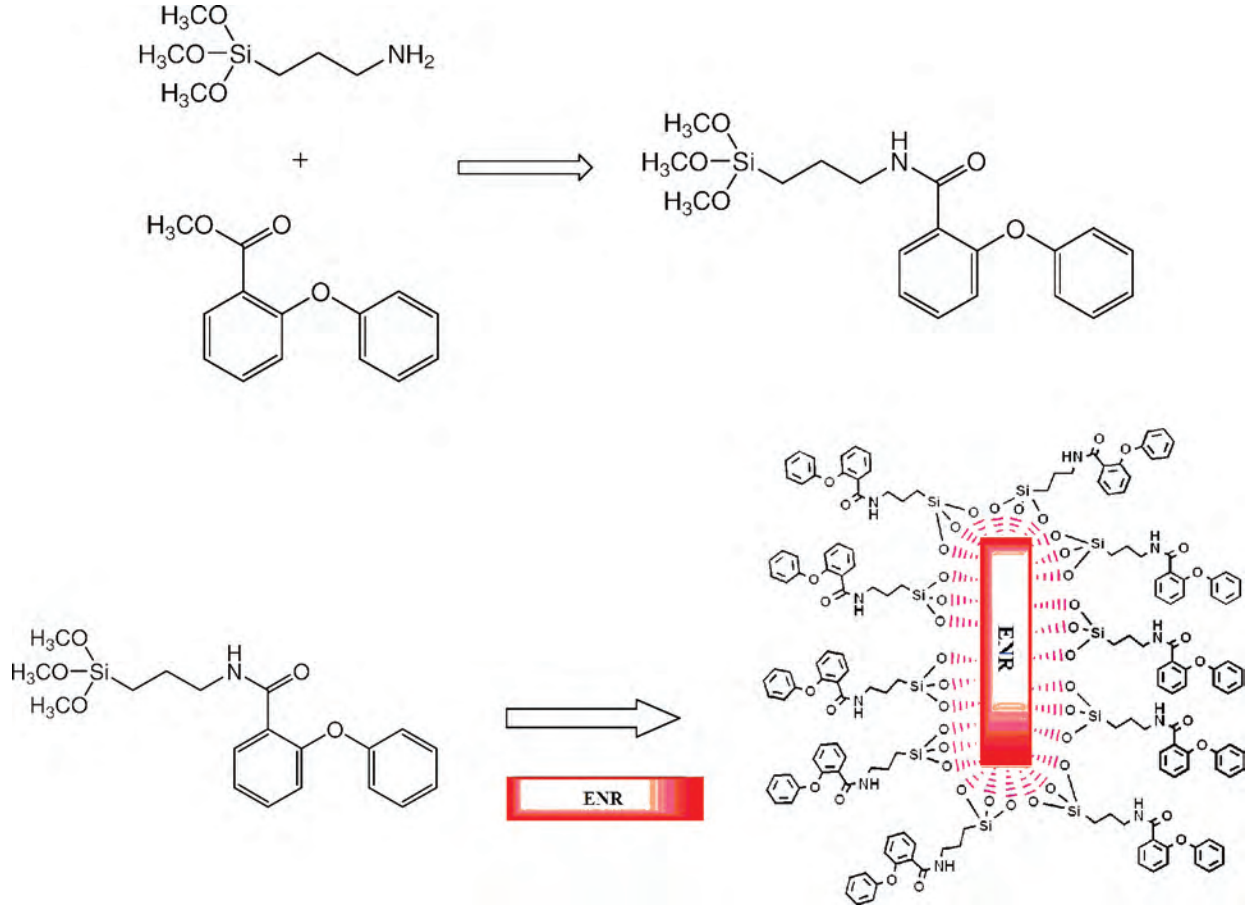

amorphous $Eu(OH)_3$,[31] and it is very similar to part c of Figure 3. More careful control of the synthesis conditions would enable purer-phase material to be produced. Note that the spectra shown in parts b and c of Figure 3contrast the different line widths available in potential applications for cell imaging at cryogenic temperatures. The 10 K emission spectrum of FENR under 457 nm excitation shows very broad features (part d of Figure 3), just as in part b of Figure 3, but the sharper bands in the latter due to $Eu(OH)_3$ are absent.

The absorption spectrum of the functionalized ORMOSIL coating (Figure S3, Supporting Information) exhibits strong absorption bands at 330 nm (30 303 cm^{-1}) and 390 nm (25 641 cm^{-1}), which are attributable to the $\pi \rightarrow \pi^*$ transitions. The low-resolution room-temperature emission

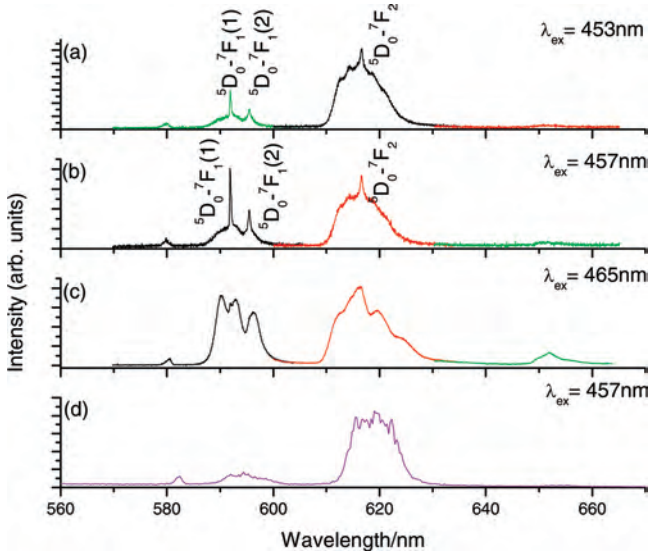

Figure 3. 10 K luminescence spectra of (a) ENR at λ_{ex} = 453 nm; (b) ENR at λ_{ex} = 457 nm; (c) ENR at λ_{ex} = 465 nm; and (d) FENR at λ_{ex} = 457 nm.

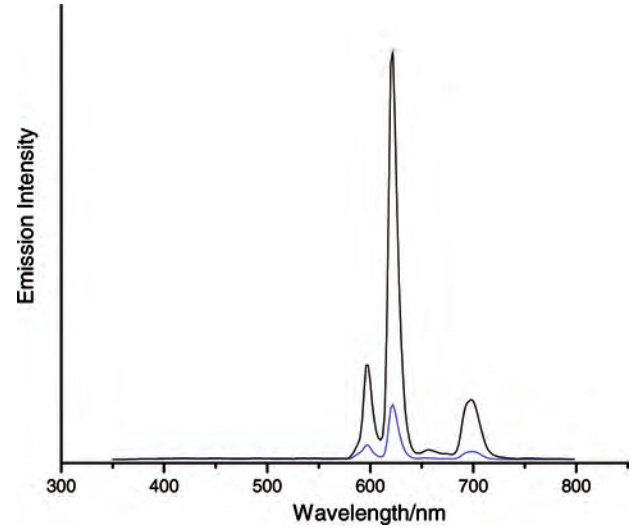

Figure 4. Enhancement of the red $^5D_0$ emission from the ENR (blue line) by surface functionalization by sol−gel silica with chemically bound chromophores (black line) (λ_{ex} = 390 nm).

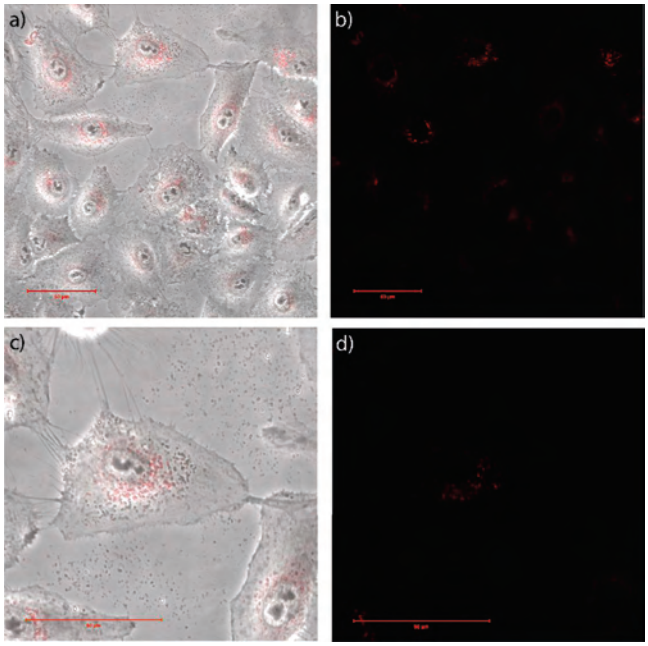

Figure 5. Confocal fluorescence microscope images of human lung carcinoma A549 cells loaded with ENR (10 μg ml^{-1} complex concentration in the growth medium) after 24 h revealing the red Eu^{3+} emission above 570 nm (λ_{ex} = 458 nm). (a), (b) Bright-and dark-field images, respectively, show the morphology of the red staining of the cytoplasm by the nanorods (20×); (c), (d) red staining of ENR in a single cell (60×).

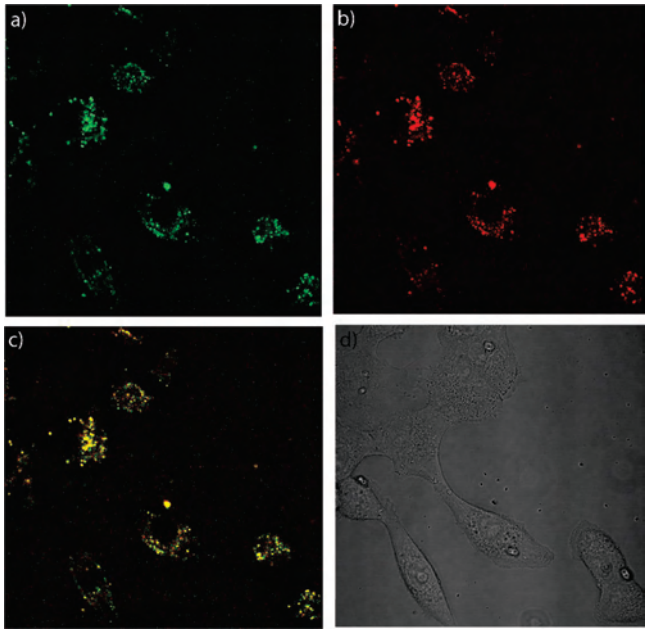

Figure 6. Confocal fluorescence microscope images of human lung carcinoma A549 cells after 6 h of exposure to: (a) fluorescent dextran (Alexa Fluoro 488, λ_{ex} = 488 nm); (b) ENR (λ_{ex} = 457.9 nm); (c) costaining image (10 μg ml^{-1} complex concentration in the growth medium); (d) Bright-field image.

spectrum (Figure 4) shows the enhancement of $^5D_0$ emission bands under 390 nm excitation of the FENR compared to that of the ENR. This enhancement is obviously attributable to the energy transfer from the antenna chromophores of the surface functionalized ORMOSIL coating to the Eu^{3+} in the nanorods. Furthermore, larger quantum yield (FENR: 0.11; ENR: 0.02) and longer lifetime (FENR: 1.97 ms; ENR: 0.56 ms) are observed in the solid-state FENR with the same excitation at 390 nm.

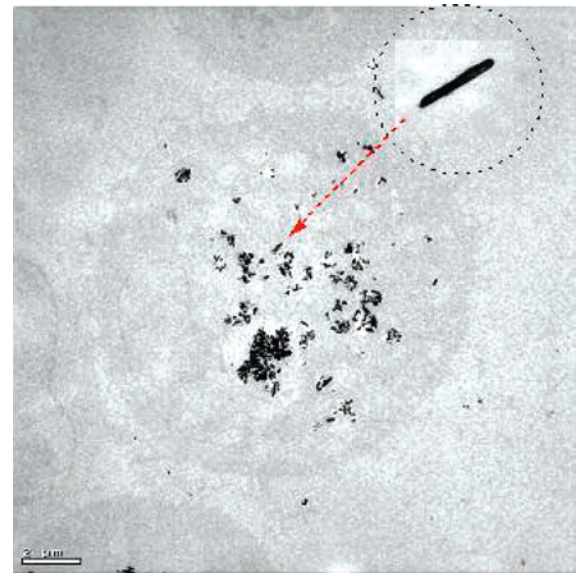

Figure 7. TEM image (80 kV) of the distribution of the internalized ENR inside an A549 cell.

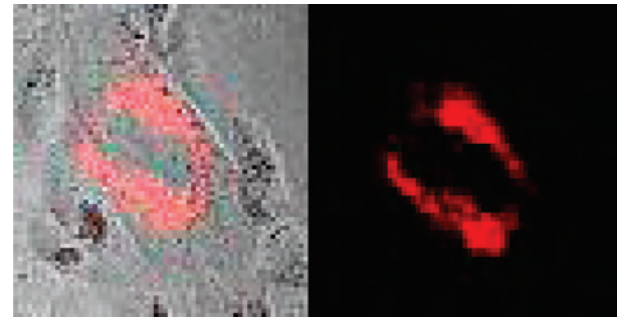

Figure 8. Fluorescence microscope images of human lung carcinoma A549 cells exposed to FENR showing the red Eu^{3+} emission above 600 nm. (6 h exposure; 5 μg nanorods ml^{-1} of the growth medium; λ_{ex} = 400 nm; filter bandpass for λ_{em} = 600−650 nm).

Internalization of the bare and functionalized europium nanorods in human lung carcinoma A549 and Hela cells were studied at the nanorod loading of 10 μg ml^{-1} over an exposure period from 30 min to 24 h. Cells loaded with these two types of nanorods were excited at 390 and 457.9 nm. For the ENR, pale-red luminescence areas were observable in the cytoplasm of a small number of cells after 2 h of exposure (part a of Figure S4, Supporting Information). After a further 2 h, more cells were found to give pale-red luminescence in the cytoplasm and especially around the nucleus (part b of Figure S4, Supporting Information). At an exposure time of up to 6 h, red luminescence was observed around the nucleus of most of the cells (not shown). No emission was observed inside cells that were exposed to comparable concentrations of commercial $EuCl_3$ or Eu_2O_3 as controls (Figure S5, Supporting Information), where only dark spots were observed outside the cells. Figure 5 shows the ENR staining around the nucleus increased to its maximum after 24 h of exposure. The localization of ENR was examined with green staining by the commerial cytoplasm marker (fluorescent dextrans Alexa Fluoro 488, part a of Figure 6) with excitation at 488 nm, at which Eu^{3+}

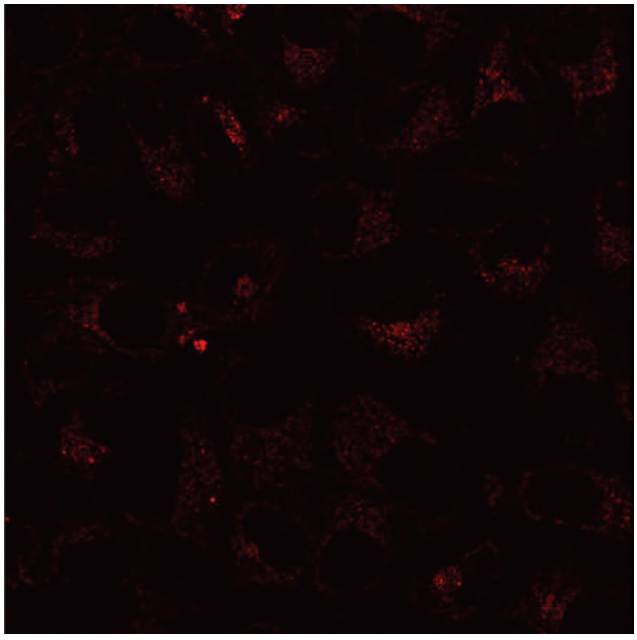

Figure 9. Confocal fluorescence microscope image of Hela cells exposed to FENR (conditions as in Figure 8).

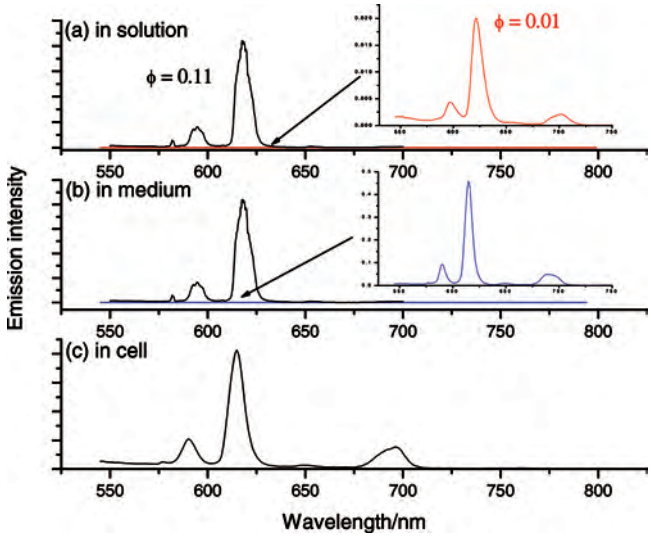

Figure 10. Room-temperature luminescence spectra of the FENR and ENR (inset): (a) aqueous solution emission spectrum in the range 550−675 nm; (b) emission spectrum of a suspension in the cell culture medium; (c) confocal microscope emission spectrum from A549 cells loaded with FENR (λ_{ex} = 390 nm). The apparent wavelength shift in (c) is due to calibration error of the microscope.

cannot be directly excited. By contrast, the red emission in part b of Figure 6 is induced by ENR with excitation at 457.9 nm. The overlapped stainings are shown in part c of Figure 6 with simultaneous excitation at 457.9 and 488 nm. The bright field image of the examined A549 cells is shown in part d of Figure 6. In addition, A549 cells with internalized ENR were examined by TEM. Figure 7 unambiguously illustrates the internalization of the nanorods within the cytoplasm, but not in the nucleus, of A549 cells.

Similar results were observed in the internalization of FENR in A549 and Hela cells (Figures 8 and 9). A red

(30) Feofilov, S. P.; Kaplyanskii, A. A.; Zakharchenya, R. I.; Sun, Y.; Wang, K. W.; Meltzer, R. S. *Phys. Rev. B* **1996**, *54*, R3690.

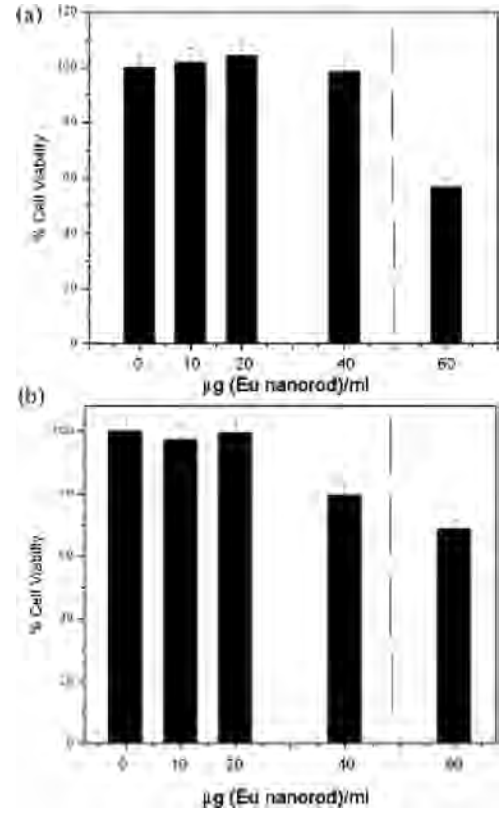

Figure 11. MTT assay for cytotoxicity of (a) ENR and (b) FENR in Hela cells. The dosed concentrations for imaging fall to the left of the dashed line.

emission was not observed inside the nuclei. However, the red emissive stainings inside the cytoplasm are much stronger under 400 nm excitation due to the antenna effect of the coating. As the chromophores in the ORMOSIL coating are chemically bound, they do not contribute any additional cytotoxicity to the nanorods, and cells were found to survive with the FENR staining over a period of 24 h.

Figure 10 shows that the room-temperature luminescence spectra of the FENR and ENR localized in cells exhibit a similar $(^5D_0 \rightarrow {}^7F_2)/(^5D_0 \rightarrow {}^7F_0)$ intensity ratio of the bands at 618 and 580 nm in aqueous suspension and in the cell culture medium. This demonstrates that the integrity of these two kinds of nanorods before and after entering the cells.

Observations on cells exposed to the ENR as well as FENR for over 24 h did not show any apparent cytotoxicity from MTT assays (Figure 11).

Conclusions

In summary, we have reported a hydrothermal method for the synthesis of europium hydroxide nanorods and then performed their surface functionalization by a phenoxybenzoate chromophore-containing ORMOSIL coating. Both of the bare and functionalized europium hydroxide nanorods were able to stain the cytoplasm of living human cells and reached maximal staining at 24 h. The functionalization of the europium hydroxide nanorods resulted in an enhancement of the red $^5D_0$ emission from Eu^{3+}, both in the solid state and in vitro. The low cytotoxicity of the antenna-coated europium nanorod material and its luminescence properties

render it to be a potential candidate for cell imaging and targeted drug delivery. Further assessments on the in vivo toxicity of these nanorod materials are underway to evaluate their applicability in whole organism/tissue imaging.

Acknowledgment. The work described in this article was funded by grants from City University of Hong Kong (Project Nos. 7002002 and 7002087). K.L.W. acknowledges the Research Enhancement Scholarship Scheme from City University of Hong Kong.

(31) Chen, G.; Haire, R. G.; Peterson, J. R. *J. Phys. Chem. Solids* **1995**, *56*, 1095.

Supporting Information Available: EDX of ENR and FENR, and photos of control experiments. This material is available free of charge via the Internet at http://pubs.acs.org.

IC8000416